Journal of
Marine Science and Engineering

MDPI

Article

Influence of Structure and Liquid Limit on the Secondary Compressibility of Soft Soils

Nan Jiang [1], Changming Wang [1,*], Qian Wu [2] and Shuo Li [1]

1 College of Construction Engineering, Jilin University, Changchun, Jilin 130026, China; jiangnan17@mails.jlu.edu.cn (N.J.); shuoli1992@163.com (S.L.)
2 School of Highway, Chang'an University, Xi'an 710064, China; wuqian@chd.edu.cn
* Correspondence: wangcm@jlu.edu.cn

Received: 29 July 2020; Accepted: 14 August 2020; Published: 19 August 2020

check for updates

Abstract: The macroscopic mechanical properties of natural sedimentary soft soils, which are usually linked to their microstructure, are different from those of remolded soils. The interaction between soil structure and mechanical behavior is a manifestation of structural mechanics effects. It is essential to understand the effects of secondary compressibility to predict long-term foundation deformations. The effects of soil composition on secondary compression deformation are little studied, and the soil structure is rarely involved in the compression process. The sedimentary environment creates the initial composition and structure of soft soil, and it also basically determines its grain size and mineral composition, while different depths give soft soil different overburden pressures, and the soil composition and depth directly affect its yield stress during compression. So, natural sedimentary soft soils sampled at different depths and from different sedimentary environments (such as marine-neritic facies, sea shore facies and limnetic facies) were selected to study the influence of structure on the secondary compression coefficient C_α during pressure change and the relationship between soil composition and C_α. One-dimensional compression and consolidation creep tests were carried out on undisturbed and remolded samples. The undisturbed samples were obtained by the thin-wall samplers in rotary wash borings, and the quality of the samples met the test standard. Based on the concept of the void index I_v and the intrinsic compression line (ICL) proposed by Burland, the role of structure in the compression process was studied, and the influence of soil composition and structure on secondary compression characteristics was summarized. The C_α/C_c values are 0.031, 0.034, 0.030, and 0.036 for Shanghai, Tianjin, Suzhou, and Ningbo soft soils, respectively, within the range of inorganic clays and silts (0.04 ± 0.01) given by Mesri. According to the compression index C_c obtained by compression test, C_α/C_c can be used to estimate C_α. The yield stress of normal consolidated soil is near pre-consolidation pressure, while that of structural soft soil is greater than its pre-consolidation pressure. Natural sedimentary soft soils show over-consolidation characteristics due to the action of the structure; the soil structure resists the external load and hinders secondary compression. When the soil structure is almost destroyed, the pressure reaches the structure full yield stress P'. The tests of structural soft soils show that C_α changes with pressure before the structure completely yields, first increasing and reaching peak $C_{\alpha max}$ near P'; the value of P' is approximately 1.6–3.0 σ'_k, where σ'_k refers to the structure yield stress of soil obtained by the Casagrande method. After the structure disappeared, C_α gradually decreased and then stabilized, which is considered to be independent of the load. The $C_{\alpha max}$ is positively correlated with the liquid limit, indicating that the peak value that can be reached by the C_α is related to the maximum content of bound water in soft soil, thus the soil composition has a significant influence on secondary compressibility, which contributes to the prediction of long-term foundation deformation.

Keywords: soft soil; secondary compression; soil composition; intrinsic compression line; structure full yield stress; liquid limit

1. Introduction

Soft soils are widely distributed all over the world and are found in coastal areas and round rivers and lakes. For example, there are deep soft soils in North America, Northern Europe and Southeast Asia [1–3]. Soft soil has the engineering properties of low shear strength, high compressibility and low permeability, and its compressibility is the key parameter determining the deformation law of a foundation. Soil compressibility is reflected in two aspects: as the excess pore water pressure dissipates, the effective stress increases, and the compressive deformation is the primary consolidation deformation of the soil. After the excess pore water pressure is completely dissipated and the effective stress becomes basically stable, the bound water film on the surface of the soil particles creep and the rearrangement of the soil structure leads to the secondary compression deformation of the soil [4].

Many secondary safety problems and engineering hazards are caused by secondary compression deformation. The Italian Leaning Tower of Pisa is caused by excessive uneven settlement due to secondary compression deformation of its foundation. Built in 1904, the Mexico City's Art Palace is located on 25-m-thick soft soil. The ultrahigh compressibility of this soft soil is rare, with natural moisture content between 150% and 600%, and the highest void ratio is 12. Since its establishment, its settlement has been as much as 4 m [1]. Therefore, the study of secondary compression deformation is very important in engineering construction. With the improvement in the requirements for postconstruction settlement of soft soil foundations in actual engineering, the role of secondary compression and its influencing factors have attracted wide attention.

As a multiphase medium, soft soil's properties are closely related to the soil composition and structural characteristics. Currently, research on the secondary compression deformation law of soil is mainly focused on the influence of pore moisture content, load, loading history and loading time on secondary compression [5–10]. There have been some studies on the effects of different soil compositions on the secondary compression characteristics. Mesri summarized the relationship between the secondary compression coefficient C_α and the compression index C_c of 22 geotechnical materials [11–13]. The primary minerals are often the main components of the silt fraction, mainly including quartz and feldspar, which are resistant to weathering. The secondary minerals are mainly composed of clay minerals, including illite, kaolinite, chlorite, and illite–smectite mixed layers. The illite–smectite mixed layers and illite are relatively hydrophilic, and the bound water content is high, which has a great influence on the creep properties of soft soil. The mineral composition and content have important influences on the physical and mechanical properties [14–16]. To study the influence of mineral composition and content on the one-dimensional compressibility of soft soil, soil samples mixed with some secondary minerals and silt have been examined, such as in research on the compressibility of different proportions of kaolin, illite and silty sand mixtures, as well as on the influence of several mineral component content on the compression characteristics; furthermore, the compressibility of kaolin and montmorillonite were compared [17–19]. However, most research is based on the compressibility of remolded soil. The understanding of the influence of the composition of undisturbed soil on the secondary compression characteristics is not sufficiently comprehensive.

The prediction method for the secondary compression coefficient C_α proposed by Mesri is the most famous for the empirical relationship between ratio of the C_α and the compression index C_c [11–13]. The slope of the curve in the secondary compression stage of the one-dimensional compression curve is C_α, and this secondary compression coefficient can be determined according to the compression index C_c of the soil [13]. In 1967, Bjerrum proposed the isochronous e–lg$p$ curve, which is used to calculate the secondary compression deformation of remolded soil [20]. These studies, based on remolded soils, suggest that the secondary compression coefficient of the soil does not change with time. Regarding the relationship between the secondary compression coefficient C_α and pressure, Bjerrum and Newland believed that it is independent of consolidation pressure [20,21]. Horn and Lambe considered that the secondary compression coefficient is independent of the incremental ratio of the load but depends on the final consolidation pressure [22].

Another view is that the secondary compression coefficient C_α is related to pressure. It was found through experiments that as the pressure increases, the value of C_α increases from small to large and then decreases [23]. For example, it was found by studying Hangzhou undisturbed clay that when the pressure was less than a certain value, the secondary compression coefficient increased with the pressure, and when the pressure was greater than this certain value, the secondary compression coefficient did not change with the pressure, but this certain value was not well defined [24]. According to the research of Lei et al., on undisturbed marine soft soil in Tianjin, the secondary compression coefficient C_α is related to pressure, and they pointed out that the boundary point of the pressure is the pre-consolidation pressure [25]. The secondary compression is related to the pressure when the soil is in the over-consolidated state and it is independent of the pressure during normal consolidation [26].

The above viewpoints and conclusions are reasonable and applicable under specific conditions, with more extensive research on secondary compression, the viewpoint that C_α varies with the consolidation pressure has been widely accepted, but there is no uniform and powerful conclusion on the load boundary points of C_α related to the pressure. The effect of soil structure on secondary compression and the relationship between structure and pressure are still worth studying.

Naturally deposited soft soils are affected by the structure during and after the deposition process. It has been well documented that such deposits behave differently under disturbed or remolded conditions [27–30]. This behavior difference results from structural resistance. The influence of the soil structure mainly refers to cementation, thixotropy, hardening, time effect eluviation and the rate of sedimentation [31,32]. Hattab et al. thought that the presence of soil structure could lead to an overestimation of the pre-consolidation pressure [33]. It was emphasized that the soil structure is the core of the development of geotechnical engineering in the 21st century [34]. For normal consolidated soil, the maximum load experienced historically is the self-weight stress, and so the yield stress of normal consolidated soil is near the pre-consolidation pressure. However, it was found that for some natural sedimentary soft soils, the yield stress is significantly greater than the self-weight stress, showing over-consolidation characteristics [35]. This is due to the effect of soil structure on mechanical properties. The soils with this performance are called structural soft soils [36]. The pre-consolidation pressure obtained by the Casagrande method is called the "structure yield stress" of the structural soil. The "over-consolidation ratio" is the "structure stress ratio" [37].

Yang et al. described the compression behavior of structural soils based on comparisons in a series of experiments on undisturbed and remolded soils [38]. The mechanical properties of naturally deposited structural soils are often different from those of remolded soil; the soil structure almost disappears when the pressure exceeds a certain value, the properties of the soils are similar to those of remolded soils at this time, and C_α is similar to that of remolded soil, but the change in C_α is worth discussing when the pressure is less than this value and the relationship between this value and the soil sample is not explained [39,40]. Mesri noted that structural failure of natural soft soil mainly occurred in the pressure range of 0.7 to 2.0 σ'_k, which means that the soil structure was almost completely destroyed when the pressure was 2.0 σ'_k [41]. However, the change in C_α is worth discussing when the soil structure is not completely yielded.

The C_α of structural soft soil is closely related to the stress level and time [11,12]. Marine sedimentary structural soil is different from the normal over-consolidated soil; the soil structure resists the external load and hinders secondary compression [42–44]. A secondary compression deformation calculation model considering the effects of the soil structure was established [45].

In the present study, natural sedimentary soft soils from Shanghai, Tianjin Suzhou and Ningbo were selected and one-dimensional compression and creep tests were carried out on undisturbed and remolded samples. The undisturbed samples were well obtained from thin-wall tube samples, meeting the test requirements, and based on their initial void ratio and the initial moisture content, the remolded samples were prepared by using sieved dry soil and distilled water to disrupt the structure of the soil (such as the influence of cementation, thixotropy, hardening, time effect and eluviation). The influence of soil composition, especially its structure, on the compressibility and secondary compression characteristics of naturally deposited soft soil was explored.

The objectives of present study were to investigate the one-dimensional compressibility, especially secondary compression behavior, and the soil structure effects of four clays obtained from Shanghai, Tianjin, Suzhou and Ningbo in China and compare the measured results with those of other natural soft soils worldwide. These four cities are relatively developed and densely populated, and the study of long-term foundation deformations is very important there. The soft soils in the four sites were selected from different sedimentary environments and depths, giving them different structural strength and yield stress. The different sorting degrees during the deposition process made the grain composition of the soft soils at these four sites different. The influence of structure and water–physical properties, such as liquid limit, on the secondary compressibility of soft soils was studied. The specific properties are described below.

2. Soft Soils and Methods

2.1. Geological Setting and Sampling

The investigation in the present study was carried out on undisturbed samples retrieved from areas of Tianjin, Shanghai, Suzhou and Ningbo, as shown in Figure 1. Tables 1–4 give the general geological conditions and sedimentary history of the four natural soft soils.

Shanghai is situated on the Yangtze River delta in eastern China, and the geology mainly consists of alluvial and marine sediments formed during the Quaternary period over the past 3 million years. The soft soil has low permeability, high sensitivity and remarkable creep properties. The Shanghai (SH) soft soil sample is from a gray muddy silty clay layer.

Most of Tianjin is a plain landform, and the southeast is bordered by Bohai Bay. The geological genesis of Tianjin (TJ) soil can be attributed to the Quaternary Holocene coastal sediment, which has the characteristics of a low bearing capacity, high compressibility and low permeability. The sample, consisting of gray silty clay, was taken from the Tianjin Airport Economic Zone.

Suzhou is located in the Taihu Lake Basin, close to the East China Sea. The soft soil is mainly composed of fluvial or limnetic sediments, with silty clay as the main part of the layer. It has the characteristics of low bearing capacity, high compressibility and a wide distribution of limnetic sediments. In present study, Suzhou (SZ) soft soil, from a gray yellow silty clay layer, was taken from the Suzhou Science and Technology City.

Ningbo is a plain landform bordering the East China Sea. The geological genesis of Ningbo soil can be attributed to the marine sediment of the middle or late Holocene, which has the characteristics of high water content, high void ratio and poor permeability. The Ningbo (NB) soft soil sample was taken from a gray yellow muddy silty clay layer.

The undisturbed samples were obtained by thin-wall samplers from the gray muddy silty clay layer, gray silty clay layer, gray yellow silty clay layer and gray yellow muddy silty clay of the SH, TJ, SZ and NB sites, respectively, in rotary wash borings, and each soil type was sampled at least 0.5 m thick. All the samples were immediately sealed on site to prevent the loss of water, packed into a sturdy wooden box, and transported to the laboratory. All care was taken to avoid disturbing the soil during sampling and transporting. According to laboratory tests, the disturbance index I_D of the four samples was within the scope of mild disturbance (0.15–0.30) [41]. The soft soils from the four sampling sites belong to grade I ($I_D \leq 0.3$), and soil of grade I can be used for all projects according to GB 50021-2001 [46].

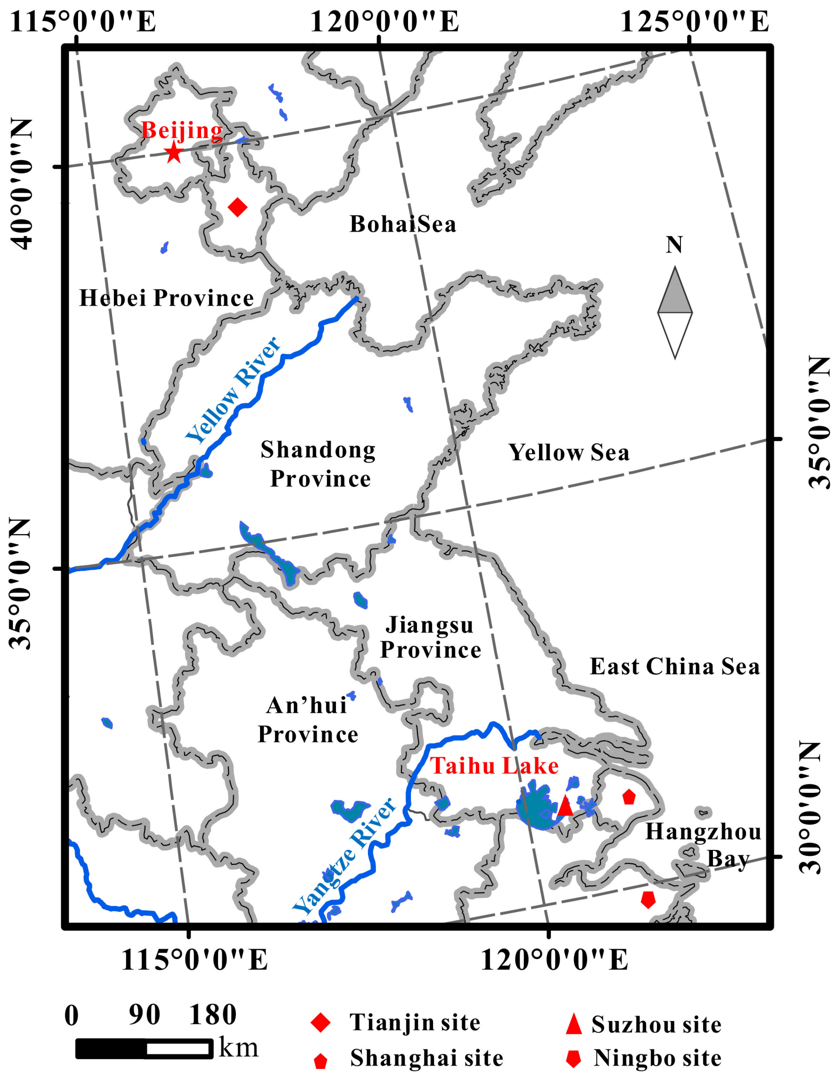

Figure 1. Sampling location of the soft soils.

Table 1. Geological conditions for Shanghai.

Chronology	Lithologic Characteristics	Core Depth (m)	Sedimentary Environment
Holocene	Brown yellow silty clay Gray muddy clay	0–3 3–5	Marine–estuarine facies
	[1] Gray muddy silty clay Clay and sand interlayer	5–25	Marine–neritic facies
Late Pleistocene	Dark green clay Yellow silty clay	25–35 35–40	Fluvial facies Marine facies

[1] Sampling layers of the Shanghai soft soils. Coordinates are 31°8′5″ N, 121°36′26″ E.

Table 2. Geological conditions for Tianjin.

Chronology	Lithologic Characteristics	Core Depth (m)	Sedimentary Environment
Holocene	Brown yellow silty clay	0–3	Fluvial facies
	Gray muddy silty clay [2] Gray silty clay	3–5 5–15	Sea shore facies
	Gray yellow silty clay	15–17	Terrestrial facies
	Brown yellow clay Brown yellow silty clay	17–20 20–25	Fluvial facies
Late Pleistocene	Brown yellow silty clay	25–30	Fluvial facies

[2] Sampling layers of the Tianjin soft soils. Coordinates are 39°1′11″ N, 117°11′42″ E.

Table 3. Geological conditions for Suzhou.

Chronology	Lithologic Characteristics	Core Depth (m)	Sedimentary Environment
Holocene	Brown yellow silty clay [3] Gray yellow silty clay	0–5 5–12	Limnetic facies
	Gray yellow silt Gray silty clay	12–16 16–20	Fluvial facies
Late Pleistocene	Brown yellow clay	20–27	Marine–neritic facies
	Green gray silty clay	27–42	Fluvial facies

[3] Sampling layers of the Suzhou soft soils. Coordinates are 31°6′21″ N, 120°35′43″ E.

Table 4. Geological conditions for Ningbo.

Chronology	Lithologic Characteristics	Core Depth (m)	Sedimentary Environment
Holocene	Gray yellow clay [4] Gray yellow muddy silty clay	0–3 3–12	Limnetic facies Marine facies
	Gray yellow silt Gray silty clay	12–14 14–22	Marine–neritic facies
Late Pleistocene	Green gray clay Gray silty clay	22–28 28–43	Marine facies

[4] Sampling layers of the Ningbo soft soils. Coordinates are 29°40′24″ N, 121°25′40″ E.

2.2. Properties of the Soft Soils

Figure 2a shows the grain size distribution curves of the SH, TJ, SZ and NB soft soils. Figure 2b shows the percentage of fractions in the four sites. The clay fraction content (<0.002 mm) of the NB is the highest, exceeding 30.0%, while those of TJ, SH and SZ are 21.8%, 17.1% and 14.6%, respectively.

The mineral content according to the results of the x-ray diffraction (XRD) analysis is shown in Figure 3. In general, the types of minerals in the soft soils in the four sites are similar. The primary mineral is quartz, which reflects the higher content of silt and fine sand fraction in the grain composition of the samples. The secondary minerals are mainly illite, kaolinite and chlorite. The secondary mineral content of the TJ, SH and SZ is 54%, 52% and 49%, respectively. The secondary mineral content of NB is higher than that of the other three sites; at a depth of 4.0 m it is up to 60%, and at a depth of 9.5 m is 56%, indicating that the weathering degree of the NB is the highest in four sites.

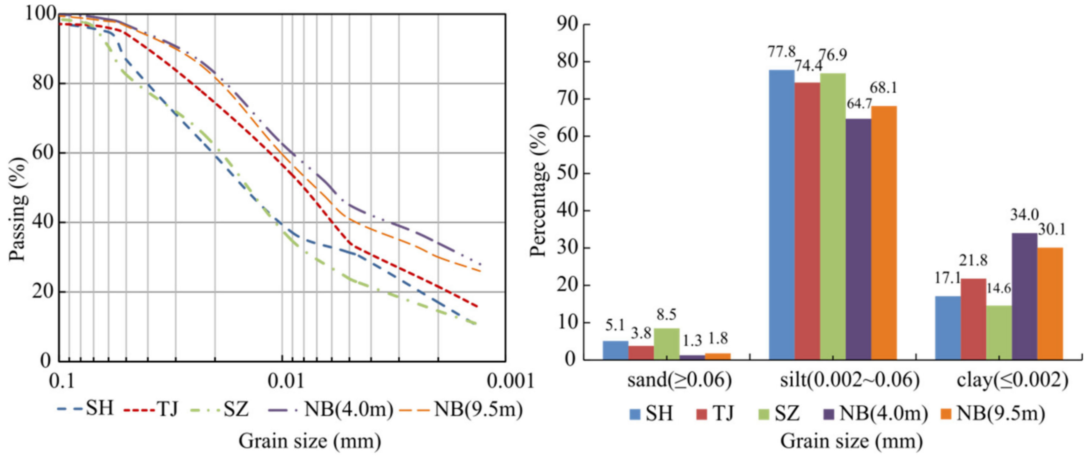

(**a**) (**b**)

Figure 2. Grain composition of soft soils: (**a**) grain size distribution curves; (**b**) percentage of mineral fractions.

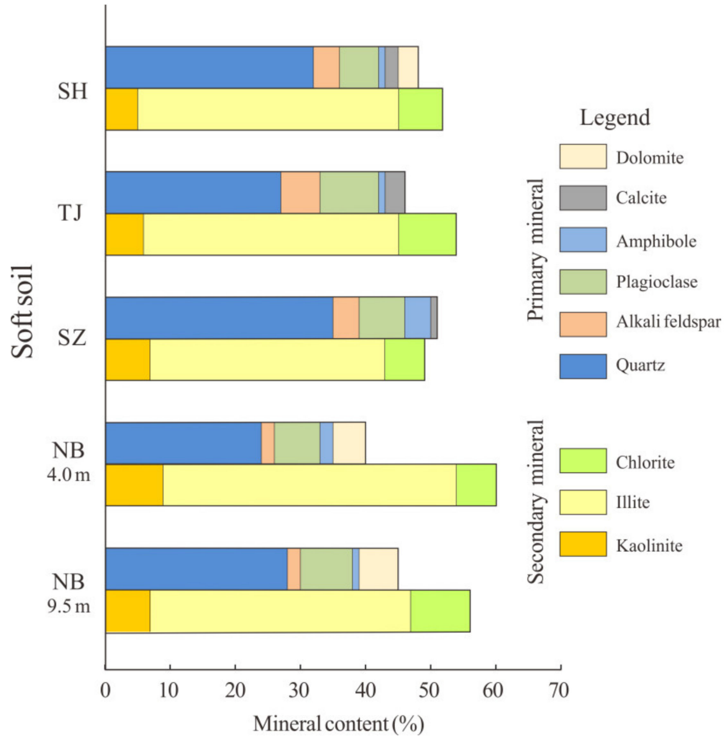

Figure 3. Mineral content of soft soils.

The physical properties of the SH, TJ, SZ and NB samples tested in the laboratory are presented in Table 5, and there are two samples at different depths in NB site. All of the soft soils are saturated. We measured the liquid limit (w_L) by the fall cone method and obtained the different fall cone depths by configuring soil samples with different moisture contents. The w_L of the soil sample was determined by using the water contents and the fall cone depths in logarithmic coordinates, and parallel samples were adopted to ensure the accuracy of the results. The liquid limits (w_L) of the NB samples are 39.2% and 42.7%, which are higher than the other three soils. The plasticity indexes (PI) of the NB samples are 18.3% and 21.1%, which are higher than the other three natural soils. The natural moisture content of the NB, TJ and SH samples is higher than their w_L, while that of the SZ sample is close to its w_L, and the w_0/w_L of SZ is 0.93. Table 5 shows that the NB sample from 4.0 to 4.5 m has the largest initial void ratio.

Table 5. Physical properties of soft soils.

Location Site	Depth (m)	Specific Gravity, G_s	e_0	w_0 (%)	w_L (%)	PI (%)	Classification (BS 5930) [47]
SH	5.0–5.5	2.65	1.25	47.0	35.4	14.0	CI
TJ	7.5–8.0	2.66	1.15	43.1	38.0	16.5	CI
SZ	10.5–11.0	2.66	0.76	28.5	30.8	12.8	CL
NB	4.0–4.5	2.70	1.33	49.3	42.7	21.1	CI
	9.5–10.0	2.67	1.07	40.1	39.2	18.3	CI

e_0: Initial void ratio. w_0: Initial moisture content.

Figure 4 shows the plasticity chart for the four soil samples on the basis of the Atterberg limits. All data are above the A-line, which is a boundary between clay and silt. According to BS 5930, the five natural soils are categorized as clays with low to intermediate plasticity [47].

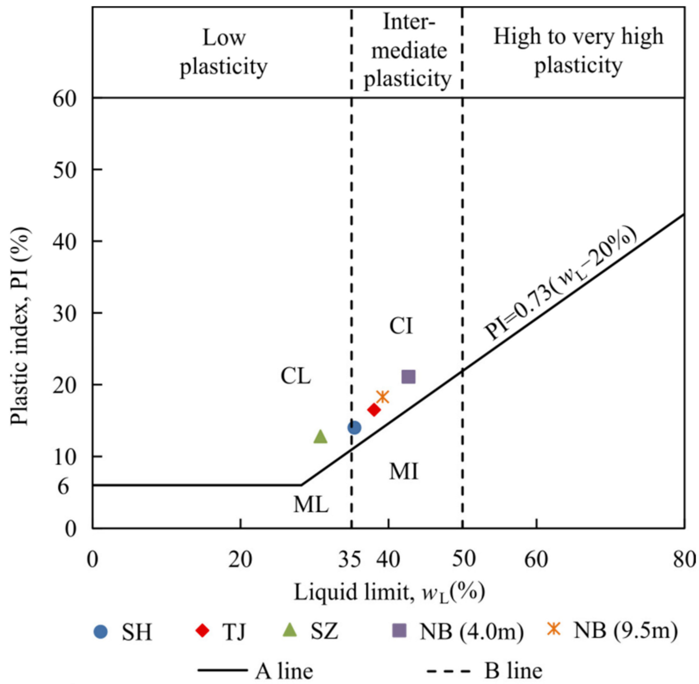

Figure 4. Plasticity chart.

2.3. Methods

Five natural soil samples were selected from different sedimentary environments or depths; the depths of the soil samples were approximately 5, 7 and 10 m from the sites of SH, TJ and SZ, respectively, and 4 and 9 m from NB. The effects on the secondary compressibility of soft soil were explored by using different clay contents, water contents and depths.

To determine the influence of soil structure on compressibility, a one-dimensional compression test was carried out on the undisturbed and remolded soil samples from the four sites. The remolded samples were prepared according to the void ratios and initial moisture contents of the undisturbed samples. To obtain the secondary compression characteristics, a one-dimensional consolidation creep test was performed on the undisturbed samples. We used a wire saw to cut off part of the soil on the surface from the thin-wall tube samples. To reduce the lateral friction between the stainless ring and the soil specimen, the inner side of the stainless ring was coated with silicone grease, then the stainless ring placed flat on the soil and gently pressed down; then we used a wire saw to cut off the soil outside the stainless ring, then continued to press down gently, repeating the operation until the stainless ring was filled with soil to obtain the undisturbed sample. We collected the cut soil, dried it to a constant weight at 105 °C, then crushed it and passed it through the sieve 10 (2 mm); depending on the initial void ratio and initial moisture content of the undisturbed sample, the required dry soil and distilled water were properly mixed by using a geotechnical blade, then the wet soil was sealed. After placing the wet soil aside for 24 h, we filled the stainless ring with a geotechnical blade according to the calculated mass of the wet soil to obtain the remolded sample. Great care was taken to control the speed during sample preparation to prevent water loss. All the tests were carried out in a temperature-controlled room (23 ± 1 °C) to minimize the effect of temperature on the consolidation tests.

The conventional consolidation instrument was used to test the undisturbed and remolded soil samples for the four sites under the condition of two-side drainage, and the samples were always in a saturated state. The diameter and height of the specimens were 61.8 and 20 mm, respectively. The consolidation rings containing the samples were placed in the consolidation cell with filter paper and porous stone on both ends of the samples.

Using a step-loading method and a load increment ratio of 1, a total of fifteen soil samples were tested in two series. Series 1, including five undisturbed samples and five corresponding remolded samples, underwent one-dimensional compression tests. Series 2, including five undisturbed samples, underwent one-dimensional consolidation creep tests. Details of the tests are summarized in Table 6. The estimated in situ vertical stresses "$\sigma_v{}'$" were shown in Table 6. The smallest $\sigma_v{}'$ of undisturbed soil was about 50 kPa, which is relatively small. In order to better reflect the compression process, reduce the load variation of the prior stage and better determine the structure yield stress of soil sample, we chose a small initial stress to be 12.5 kPa. We used a step-loading method and a load increment ratio of 1, for a total of 8 loading stages for all undisturbed soil samples. In one-dimensional compression test, all the remolded soil samples were unloaded and reloaded after 400 kPa and each stage of load was maintained for 24 h. At present, there is no definitive deformation standard for creep test; it is generally considered that the creep has reached stability when the deformation is less than 0.01 mm within 10,000 s [48,49]. According to the test situation of one-dimensional consolidation creep tests, and to avoid losing moisture during the long test time, we determined the deformation standard as follows: when the deformation of a sample was less than 0.01 mm within one day (which is longer than 10,000 s), the next stage load was applied, and the sample was loaded for three days at each stress level to meet this deformation standard, so the time of duration of load is three days for each stage in one-dimensional consolidation creep tests, which is consistent with Quigley's deformation standard [50].

Table 6. Test program.

Test Procedure	Test No.	Core Depth (m)	$\sigma_v{}'$ (kPa)	Vertical Loading Procedure (kPa)	Time of Duration (Day)
1. One-dimensional compression test	SH-1	5.2	55	12.5–25–50–100–200–400–800–1600	1
	TJ-1	7.6	85		
	SZ-1	10.6	109		
	NBI-1	4.2	48		
	NBII-1	9.6	94		
	SH*-1	5.2	55	12.5–25–50–100–200–400–200–100–50–25–12.5–0–12.5–25–50–100–200–400–800–1600	1
	TJ*-1	7.6	85		
	SZ*-1	10.6	109		
	NBI*-1	4.2	48		
	NBII*-1	9.6	94		
2. One-dimensional consolidation-creep test	SH-2	5.3	56	12.5–25–50–100–200–400–800–1600	3
	TJ-2	7.7	85		
	SZ-2	10.7	110		
	NBI-2	4.3	49		
	NBII-2	9.7	95		

3. Results

3.1. Compression Curves

Figure 5 shows the e-σ_v' curves from one-dimensional compression tests for the undisturbed and the remolded samples. It can be seen that the compression curves of the undisturbed samples had significant inflection points compared with those of the remolded samples, indicating that the soft soil used in the test had structural properties. For the naturally deposited structural soil, the pre-consolidation pressure of the soil was obtained according to the Casagrande method, called the structure yield stress σ'_k [37]. The σ'_k for samples of the SH, TJ, SZ, NBI-1 and NBII-1 are approximately 66, 95, 120, 59 and 115 kPa, respectively. Given that the estimated in situ vertical stresses σ_v' are 55, 85, 109, 48 and 94 kPa, the structure stress ratio σ'_k/σ_v' of samples SH, TJ, SZ, NBI-1 and NBII-1 are 1.20, 1.12, 1.10, 1.23 and 1.22, respectively.

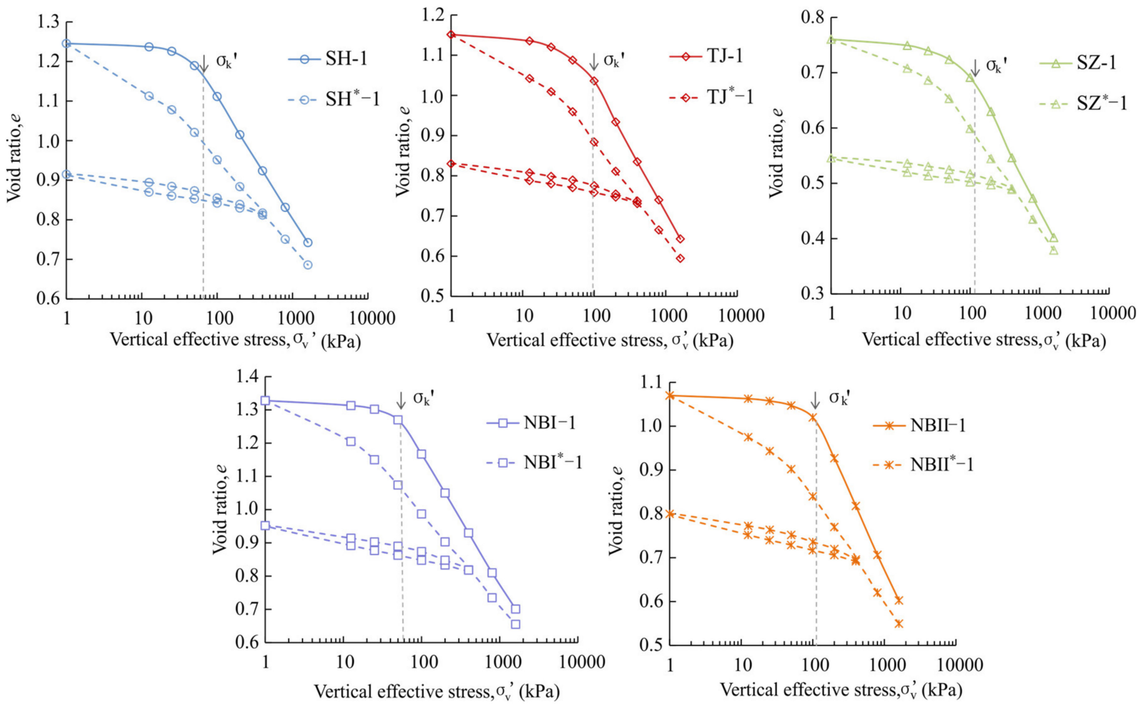

Figure 5. Compression curves for undisturbed and remolded samples.

During the initial loading increments period, the changes in the void ratios were smaller for the undisturbed samples; however, the void ratios of the remolded samples changed considerably. When the pressure increased beyond σ'_k, the curves of undisturbed samples began to steepen, and the undisturbed and remolded sample curves of each type of soil tended to merge, indicating that the initial soil structure began to break down. When the pressure exceeded 200 kPa, the compression curves were almost straight, the collapse of the structure caused the compressibility to increase sharply and the compression index C_c was obtained.

Due to the structure of the naturally deposited soft soils, when the effective stress was less than the structure yield stress σ'_k, the compressibility of the undisturbed samples was less than that of the remolded samples. At this time, the destruction of the large pores and the discharge of free water were greater. When the effective stress exceeded σ'_k, the structural failure began to develop. In addition to the slippage between the grains, there was an accompanying collapse of the structure, and the compressibility was larger than that of the remolded samples with a lower void ratio at the same pressure level.

Finally, Figure 5 shows that the curves of each undisturbed and corresponding remolded sample were very close at the pressure level of 1600 kPa, indicating that the soil structure of the undisturbed sample was greatly damaged, which was similar to that of the remolded sample. The deformation under high pressure was mainly due to the slippage between grains. A summary of the compression index C_c of the soil samples from the different sites is given in Table 7. It can be seen that the NB soil has higher C_c.

The soil structural strength q is the difference between the structure yield stress σ'_k and the pre-consolidation pressure, which intuitively represents the size of the soil structure. However, it is difficult to determine the pre-consolidation pressure of structural soil. Based on the research of Casagrande and Schmertmann et al., Li and Zou used the rebound and recompression of remolded soil to establish a reduced compression curve based on the disturbance soil model, and obtained the pre-consolidation pressure of structural soil [51–53].

The model of the reduced compression curve is as follows:

$$\begin{gathered} e = e_1 - C_r(\lg P_L)^{1-A}(\lg P)^A, \\ A = 1 + \frac{\lg(\frac{C_s}{C_r})}{\lg\frac{\lg\sigma'_k}{\lg P_L}} \end{gathered} \tag{1}$$

where e_1 is the corresponding void ratio at a pressure of 1 kPa, which can be replaced by the initial void ratio e_0; C_r is the compression index of the ideal remolded sample, that is, the slope of the ideal remolded sample compression line; C_s is the rebound index of the remolded sample, that is, the slope of the connection line of the rebound hysteresis loop of the remolded sample; σ'_k is the structure yield stress of the original sample; P_L is the pressure value corresponding to the intersection point of the compression curve of the remolded and undisturbed sample; and A is the reduction coefficient, which reflects the characteristics of the reduced compression curve.

Figure 6 shows the reduced compression curve [51]. The structural strength q of the sample was determined by this method, and the pre-consolidation pressure results and mechanical parameters are summarized in Table 7. It can be seen that the pre-consolidation pressure and the in situ vertical stress "σ_v'" of each soil sample are very similar, indicating that the five natural soil samples are normally consolidated soft soil. It shows that the structural strength q of SH and NB is greater than 10 kPa, which is higher than that of the other two samples.

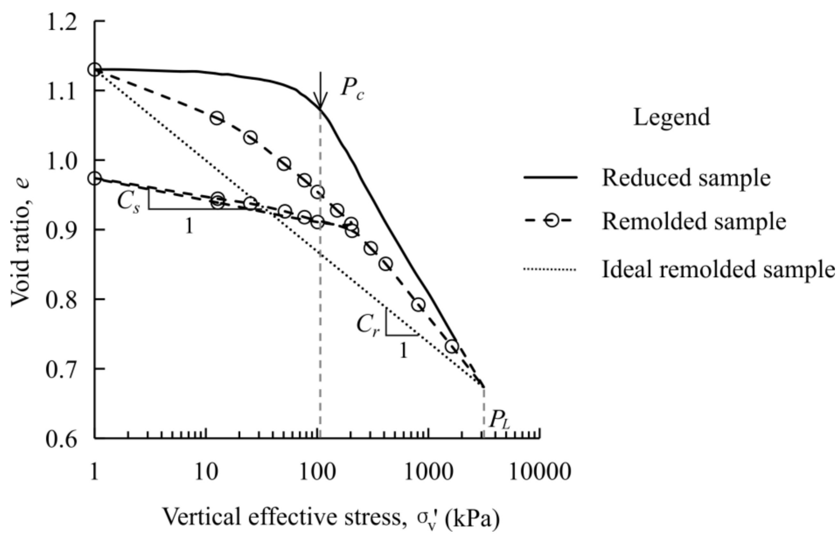

Figure 6. The reduced compression curve after [51].

Table 7. Parameters of one-dimensional compression tests.

Test Sample	Structure Yield Stress, σ'_k (kPa)	C_c	C_s	C_r	P_L (kPa)	Pre-Consolidation Pressure, P_c (kPa)	Structural Strength, q (kPa)
SH	66	0.306	0.03	0.17	4100	55	11
TJ	95	0.326	0.02	0.12	3350	86	9
SZ	120	0.240	0.03	0.18	3300	113	7
NBI	59	0.375	0.04	0.22	3100	49	10
NBII	115	0.345	0.03	0.17	3000	95	20

3.2. Creep Curves

Figure 7 shows the e-lg$t$ curve under various loadings on the basis of the one-dimensional creep test. When the pressure is small, the e-lg$t$ curve was very smooth, with no obvious boundary between primary consolidation and secondary compression. When the pressure increased beyond σ'_k, the curves presented a typical inverse S-shape, with a relatively obvious boundary between primary consolidation and secondary compression and a significant increase in creep deformation. At this time, the soil structure began to break down, and the secondary compression effect was visible, the curve showed a typical creep process. At higher loading levels, the primary consolidation effect decreased gradually. When the pressure was up to 1600 kPa, such as in the SZ creep curve, the boundary of primary consolidation and secondary compression was not so obvious.

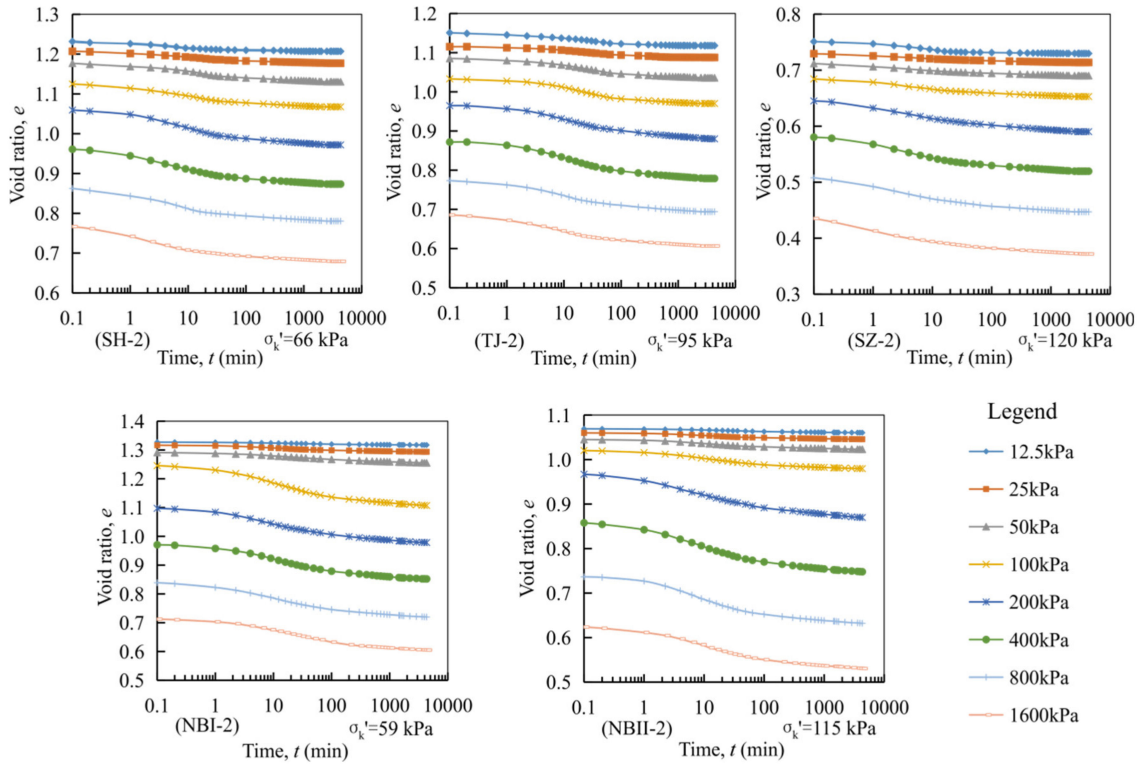

Figure 7. e-lg$t$ curves of the one-dimensional consolidation creep test.

The inverse S-shape consists of a parabola in the front, a skew line in the middle, and a gentle straight line at the end. According to the Casagrande method, the intersection point of the skew line in the middle and the gentle line at the end is the boundary point of the primary consolidation and the secondary compression [37]. When the pressure exceeds σ'_k, soil structure is destroyed, primary consolidation and secondary compression increase and peak at a certain pressure, then with the increase of pressure, the primary consolidation effect decreases gradually. Compared with primary consolidation, secondary compression is smaller. Figure 8 shows the e-lg$t$ curves under the pressure corresponding to the maximum secondary compression coefficient. At this time, the primary consolidation effect does not decrease, the slope of primary consolidation fitted line is high, the boundary of primary consolidation and secondary compression is obvious. The abscissa t_p of the boundary point of the primary consolidation and secondary compression is the time when the primary consolidation finishes. The NBI has the maximum t_p for about 100 min, which means its primary consolidation time is longer, corresponding to finer particles, and the clay fraction content is as high as 34.0%. The slope of the curve in the secondary compression stage is C_α. The calculation formula of C_α in this paper is as follows:

$$C_\alpha = \frac{\Delta e}{\lg\left(t/t_p\right)}, \tag{2}$$

where t_p and t are the completion time of the primary consolidation and a certain time after that, respectively, and Δe is the change in the void ratio of the soil sample at the corresponding time t_p and t [54].

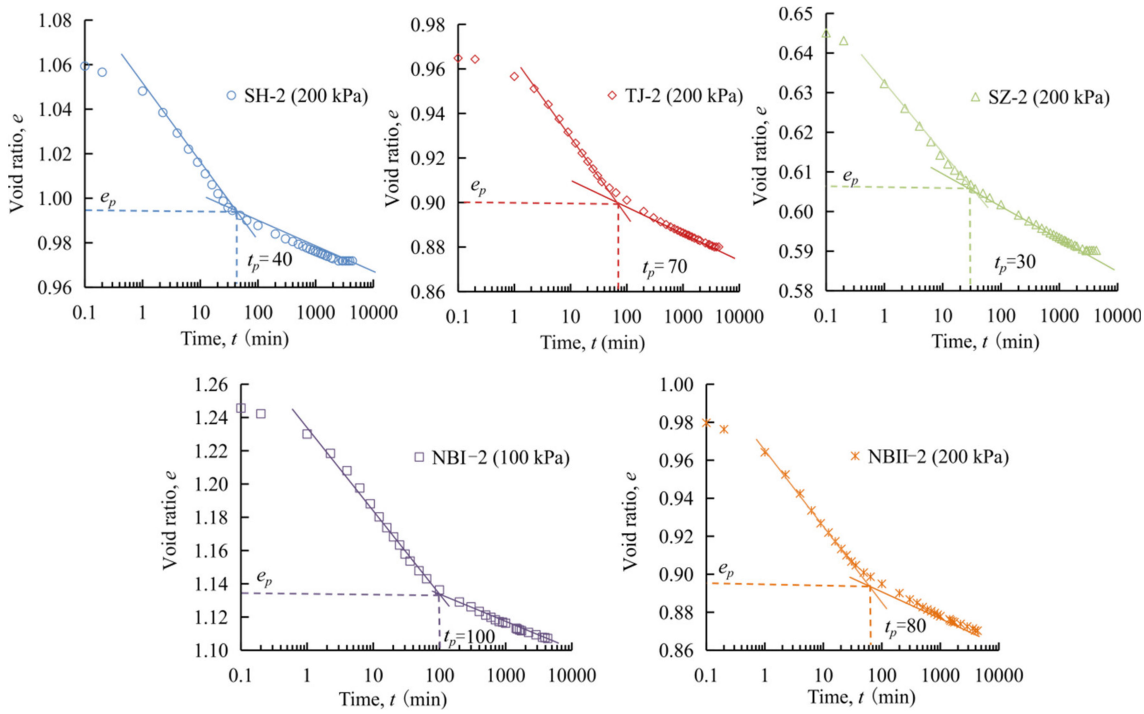

Figure 8. The e-lg$t$ curves of five samples.

4. Discussion

4.1. Variation of I_v with Pressure

Burland normalized the compression curve of remolded soil with an initial moisture content of 1.0–1.5 times the liquid limit by using the void index I_v and proposed the intrinsic compression line (ICL):

$$I_\text{v} = 2.45 - 1.285x + 0.015x^3, \tag{3}$$

where $x = \lg P$, P is the vertical effective stress (kPa), and I_v is the void index,

$$I_\text{v} = \frac{e - e^*_{100}}{e^*_{100} - e^*_{1000}}, \tag{4}$$

where e is the void ratio, e^*_{100} and e^*_{1000} are the void ratios of remolded soils with an initial moisture content of 1.0–1.5 times the liquid limit corresponding to the applied stress of 100 kPa and 1000 kPa, respectively, in the one-dimensional compression test [39].

$$I_{v0} = \frac{e_0 - e^*_{100}}{e^*_{100} - e^*_{1000}}, \quad (5)$$

where e_0 is the initial void ratio of natural deposited undisturbed soil.

Burland summarized the test data on void ratios and overburden pressures of a variety of naturally deposited undisturbed soils from various countries, and the relationship between the void index I_{v0} and overlying pressure was obtained. The natural sedimentation state of soil is mostly consistent with the sedimentation compression line (SCL), which is above the ICL. In the long-term depositional process of natural sedimentary soil, the secondary compression deformation cannot develop infinitely at the unique rate of C_α. In nature, the secondary compression deformation of most soil bodies will stop, and its sedimentary state will be consistent with the SCL.

In the one-dimensional compression tests, the remolded samples were prepared by using sieved dry soil and distilled water to disrupt the structure of the soil (such as the influences of cementation, thixotropy, hardening, time effect and eluviation), to keep other factors consistent, the moisture contents of the remolded samples were determined according to the natural moisture contents of undisturbed soils. The moisture contents of the TJ*-1, SH*-1, NBI*-1 and NBII*-1 were 1.0 to 1.3 times the liquid limit, and only the moisture content of SZ*-1 was 0.93 times the liquid limit, which basically met the conditions of 1.0–1.5 times the liquid limit. To investigate the influence of the structure of the three natural soils, the results of one-dimensional compression tests are interpreted in terms of the void index I_v proposed by Burland.

Figure 9 shows the void index I_v with the variation in the vertical effective stress σ_v' of the three samples. It can be seen that compressibility is nonlinear. Compression curves measured from the undisturbed and remolded samples are shown against the ICL and the SCL. The compression curves from the one-dimensional compression tests on the remolded samples agreed well with those predicted by Burland's equation. Therefore, we can use the ICL to analyze the compression curves.

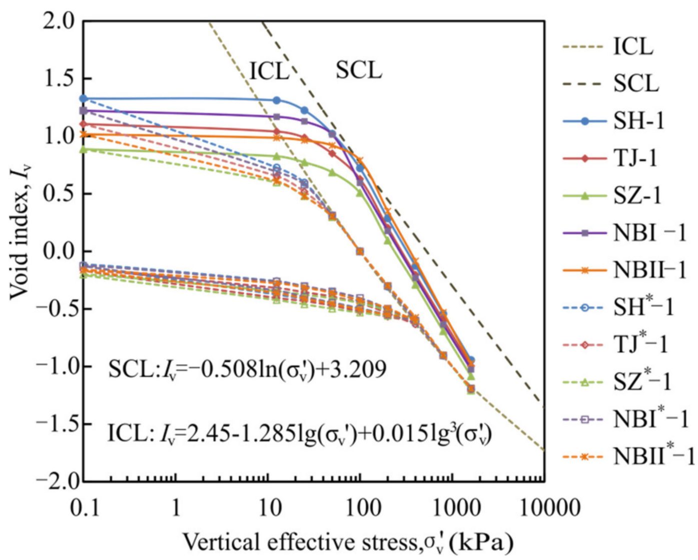

Figure 9. Void index I_v versus varied vertical effective stress σ_v'. ICL: intrinsic compression line; SCL: sedimentation compression line.

It is observed that the compression curves of all the undisturbed samples passed through the ICL at relatively low pressure and continued to stay above the ICL. The curves then approached the SCL when the vertical effective stress reaches σ'_k. The compression curve of the SH-1 touched the SCL when the vertical effective stress was around 66 kPa, the σ'_k of the SH sample. The compression curves of the TJ-1 and SZ-1 were close to the SCL when the vertical effective stresses were close to 95 and 109 kPa, which were σ'_k of the TJ sample and SZ sample. The compression curves of the NBI-1 and NBII-1 were close to the SCL when the vertical effective stresses were close to 59 and 115 kPa. When the vertical effective stress exceeded σ'_k, the curves of the undisturbed samples gradually moved away from the SCL and bent toward the ICL.

There is a void index difference (ΔI_v) between the compression curve of natural sedimentary soil and the ICL. Figure 10 shows the ΔI_v at varied vertical effective stress σ_v'. When the vertical effective stress was near σ'_k, the ΔI_v reached a peak, and then, the I_v gradually decreased with increasing pressure. The ΔI_v reached a peak when the vertical effective stress was near σ'_k, indicating that when the vertical pressure was less than σ'_k, the soil structure of the natural sedimentary soil resisted the external pressure. At this time, the soil particle skeleton was stable, the soil structure is almost unbroken, and almost no secondary compression deformation occurred. When the vertical effective stress exceeded σ'_k, the soil structure was destroyed, the I_v decreased rapidly and the ΔI_v decreased with pressure. The peak value of ΔI_v represents the structural strength of the soil, the peak value ΔI_v of NBII is relatively large, which is the largest among the five soft soils, consistent with the structural strength q calculated above.

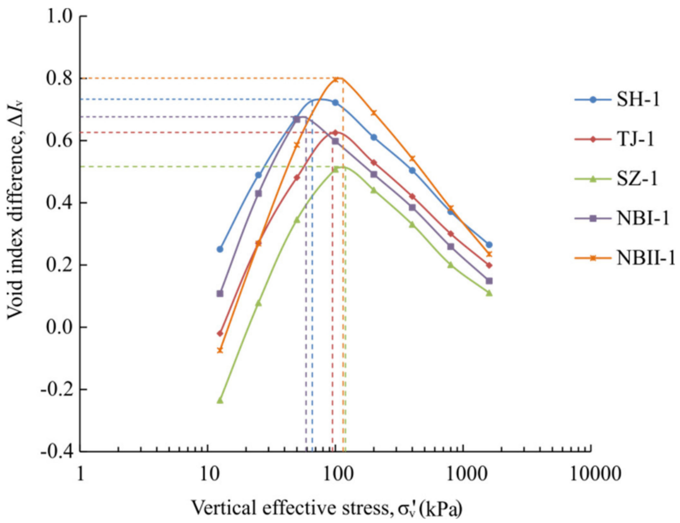

Figure 10. Void ratio difference ΔI_v versus varied vertical effective stress σ_v'.

4.2. C_α/C_c of the Soft Soils

After comparing and summarizing the test data of 22 kinds of soils, Mesri noted that for one kind of undisturbed soil, C_α/C_c is basically a constant, and the value is between 0.025 and 0.1. Table 8 shows the values of C_α/C_c for different soils [12], for example, the C_α/C_c value of fibrous and amorphous peats is 0.06 ± 0.01. According to Mesri's research, the C_α/C_c values of Middleton, James Bay and San Francisco peats are 0.052, 0.059 and 0.060, respectively, all within the range of fibrous and amorphous peats [12,13]. The soil with greater compressibility corresponds to greater C_α/C_c.

The method for determining C_α is implicit in the C_α/C_c of Mesri:

$$\frac{C_\alpha}{C_c} = \frac{\frac{\Delta e}{\Delta \lg t}}{\frac{\Delta e}{\Delta \lg \sigma_v'}} = \frac{\Delta \lg \sigma_v'}{\Delta \lg t}, \quad (6)$$

This ratio implicitly contains the influence of the soil over-consolidation degree, the soil structure and its failure on the C_α; this ratio has greatly facilitated engineering design.

Based on the experimental data, the C_α and the compression index C_c of the soft soils in the four sites were obtained. The unique linear relationships between the C_α and C_c of the soft soils were demonstrated, and the secondary compression coefficients of other typical natural clays were compared and analyzed [55]. Figure 11 shows that the C_α/C_c values are 0.036, 0.031, 0.034 and 0.030 for the NB, SH, TJ and SZ, respectively, corresponding to the slope of each fitted line, within the range of inorganic clays and silts given by Mesri. Among the soft soils in the four sites, the C_α/C_c value of the NB was the highest, corresponding to its maximum compression index.

Table 8. Values of C_α/C_c for different soils.

Material	C_α/C_c
Granular soils including rockfill	0.02 ± 0.01
Shale and mudstone	0.03 ± 0.01
Inorganic clays and silts	0.04 ± 0.01
Organic clays and silts	0.05 ± 0.01
Fibrous and amorphous peats	0.06 ± 0.01

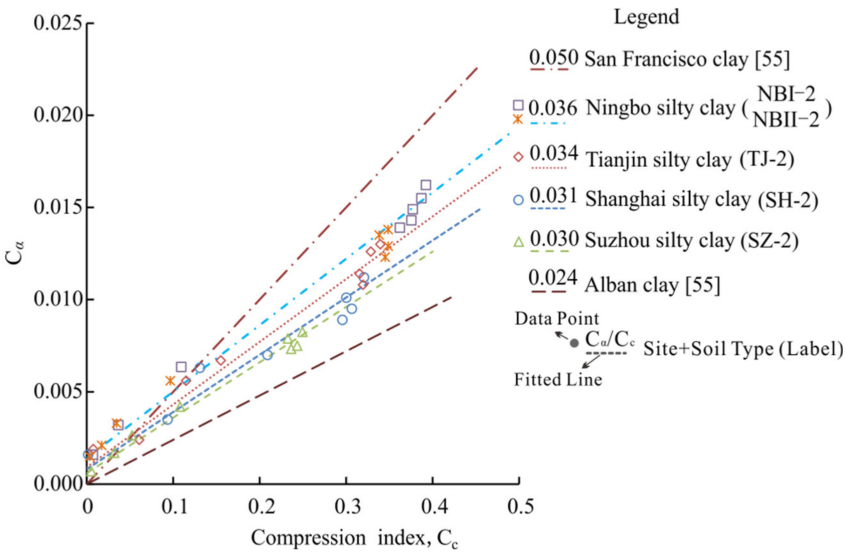

Figure 11. Comparison of C_α/C_c with other typical natural soils.

4.3. Variations of C_α with Time

In fact, the results of one-dimensional consolidation creep tests showed that the relationship of the void ratio to the logarithm of time is not a straight line and that C_α generally decreases with time [56,57]. Figure 12 shows variations of C_α with time under varied vertical effective stress for the natural clays of the four sites. It can be seen that when the pressure is less than σ'_k ($\sigma_v'/\sigma'_k < 1$), the value of C_α is low and decreases at the initial stage of secondary compression, and then is nearly unchanged over time under some pressure, such as sample NBII-2: when σ_v'/σ'_k is 0.22 and 0.43, the C_α is low and nearly unchanged over time. When the pressure is near σ'_k, the soil structure begins to break (as shown in Figures 9 and 10). At this time, the change of C_α is significant, such as in sample SH-2, when σ_v'/σ'_k is 0.76 and 1.52, respectively, C_α is much larger than when σ_v'/σ'_k is 0.38, and it becomes the highest C_α curve of SH-2 when σ_v'/σ'_k is 3.03. After the soil structure is seriously damaged, the damage process slows down and the C_α gradually decreases in stage of secondary compression, and then C_α is nearly unchanged over time under certain pressure.

In general, at low stress levels, the soil structure is hardly damaged, so C_α is low and remains almost unchanged over time. When the pressure is greater than σ'_k, C_α decreases noticeably with time. Furthermore, the value of C_α is significantly larger when the pressure is greater than σ'_k (σ_v'/σ'_k > 1), and the C_c increases accordingly at this time as shown in Figure 5. The value of C_α has to do with the structure of the soil. This is consistent with Mesri's conclusions [41]. As the vertical effective stress increases, the soil structure gradually breaks down and C_α gradually increases. After the serious destruction of the soil structure, the destruction process slows, and the value of C_α decreases at higher pressures.

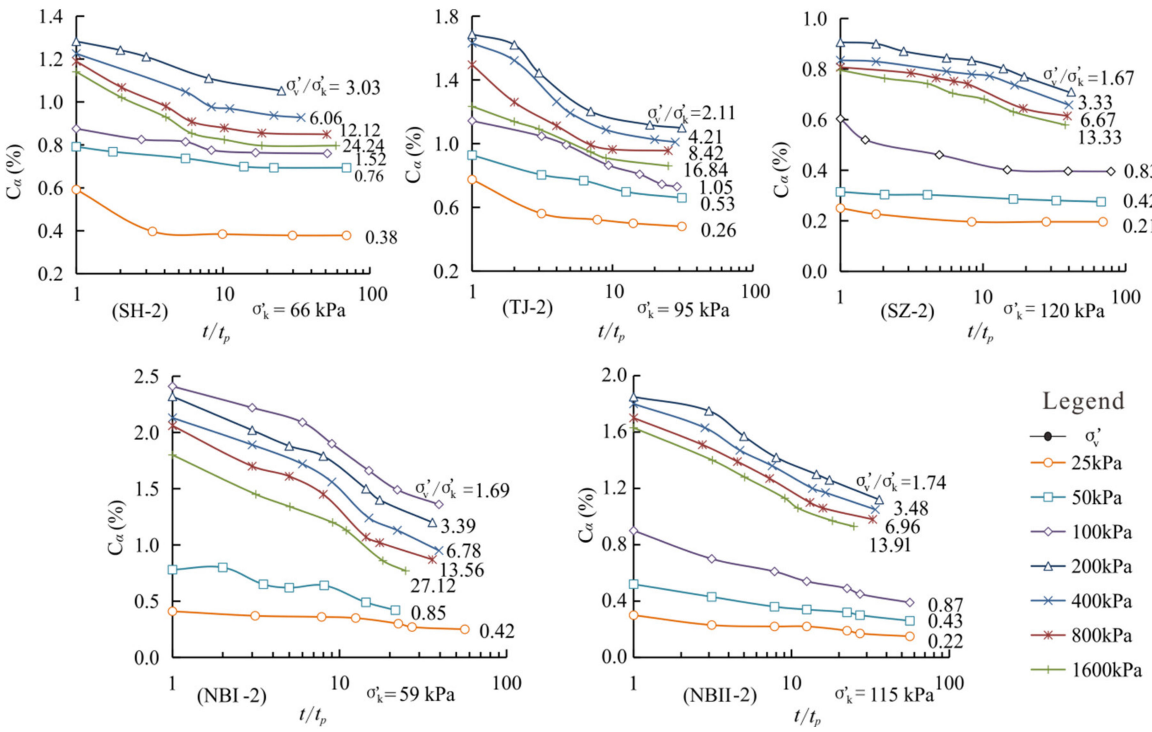

Figure 12. Variations of secondary compression coefficient C_α with time.

4.4. Relation between C_α and Pressure

Figure 13 shows variations in the measured C_α with the vertical effective stress of the five soft soils. On the whole, for each soil sample, the C_α first increased and reached a peak value then decreased with the vertical effective stress and tended to be stable. When the pressure was 12.5 kPa, the C_α of the SZ-2 was smaller compared to the other four soil samples. With the increase of pressure, the C_α of the NBI-2, SH-2 and TJ-2 increased faster, when the pressure reached 50 kPa, their C_α was significantly higher than that of SZ-2 and NBII-2. When the pressure increased to 100 kPa, the C_α of NBI-2 reached its peak, the C_α of the NBII-2 increased significantly at this time, and it exceeded the C_α of TJ-2 and SH-2 when the pressure was between 100 and 200 kPa. When the pressure was 200 kPa, the C_α of NBII-2, TJ-2, SH-2 and SZ-2 reached the peak. Finally, the C_α of each soil sample decreased with the vertical effective stress after reaching its peak and tended to be stable.

The σ'_k of NBI and SH is 59 and 66 kPa. Furthermore, the σ'_k of TJ, NBII and SZ is 95, 115 and 120 kPa, respectively. With the vertical effective stress as low as 12.5 and 25 kPa, the C_α of the five soils was small and increased slowly with pressure. The soil sample is in the pre-yield stage at this time.

When the pressure was 50 kPa, which was close to the σ'_k of NBI and SH, the C_α of NBI-2 and SH-2 increased rapidly. As shown in Table 7, NBII had the largest structural strength among the five soil samples, so the C_α of TJ-2 increased faster than that of NBII-2.

When the pressure reached 100 kPa, the C_α continued to increase, and the C_α of NBI-2 reached its peak. With the increase of pressure, the structure was in a significant destruction stage at this time and the growth of C_α was visible, especially for NBII-2. When the pressure reached 200 kPa, the C_α of SH-2, TJ-2, SZ-2 and NBII-2 reached the peak. Figure 13 shows that the $C_{\alpha max}$ of the five soft soils appeared around 100 and 200 kPa, and the C_α then decreased and tended to stabilize, called residual C_α. The residual C_α value under high pressure is 79%–89% of the $C_{\alpha max}$. Table 9 provides a summary of the secondary compression coefficient peak $C_{\alpha max}$ and the residual secondary compression coefficient $C_{\alpha r}$.

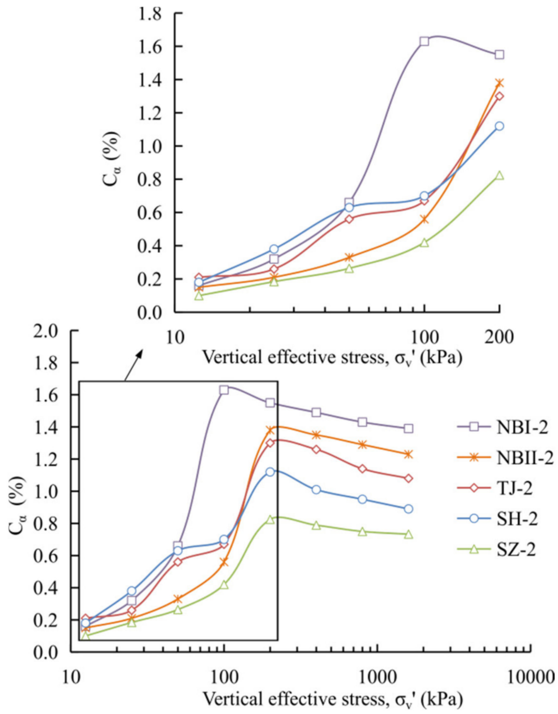

Figure 13. Secondary compression coefficient C_{α} at varied vertical effective stress σ_{v}'.

Table 9. A summary of $C_{\alpha max}$ and $C_{\alpha r}$.

Test Sample	$C_{\alpha max}$ (%)	$C_{\alpha r}$ (%)	$C_{\alpha r}/C_{\alpha max}$ (%)
SH-2	1.12	0.89	79
TJ-2	1.30	1.08	83
SZ-2	0.825	0.73	89
NBI-2	1.63	1.39	85
NBII-2	1.38	1.23	89

The test results showed that C_{α} varies with pressure [23]. According to the one-dimensional compression test, the mechanical properties of the natural sedimentary structural soft soils were different from those of the remolded soils. The soil structure also had a significant influence on the secondary compressibility; when the pressure on the soil sample was less than σ'_{k}, the soil structure resisted external pressure and was not destroyed. This stage was characterized by the destruction of large pores and the discharge of free water, and free water discharge was easier. After the primary consolidation was completed, the grain cementation hindered the sliding, and the degree of creep was small, and so the C_{α} was small at this time. When the pressure was greater than σ'_{k}, the soil structure began to fail, the collapse of the structure and the slippage between the grains readjusted the grain arrangement, the damage to the grain cementation increased the creep, and the C_{α} rapidly increased. As the pressure increased, the soil structure became increasingly weaker, and the C_{α} reached a peak. At this time, the structure was almost completely destroyed, and the compressibility of the undisturbed and remolded sample was similar. Then, it developed to a new stable condition under pressure, and the C_{α} decreased with pressure and then gradually stabilized. According to the conclusion of Zhang et al., the C_{α} of undisturbed sample under high stress was similar to that of remolded sample and did not change with pressure under high stress [43].

The structural failure of the natural soft soil mainly occurred in the pressure range of 0.7 to 2.0 σ'_k, and it can be seen that the soil structure was almost completely destroyed when the pressure was 2.0 σ'_k [41]. As shown in Figure 14, the research of Li et al. on the Shanghai soft soil at depths of 8.5 and 15.5 m, showed that the C_α changed with pressure and reached a peak after the structure yielded. The peak value appeared near 2.4 to 2.5 σ'_k, and with increasing pressure, the C_α gradually approached the value of the remolded soil [44]. Figure 13 shows that the maximum structure yield stresses of SH, TJ, SZ and NB were 3.0, 2.1, 1.7 and 1.7 σ'_k, respectively, close to the results of Mesri [41]. When the soil structure was almost completely destroyed, the corresponding stress P' was called the structure full yield stress [26,42]. Many studies obtained this result. Table 10 shows a summary of σ'_k and P' from different sites [1,23,25,44,50,58–61]. It can be seen that the P' of soft soil was greater than its corresponding σ'_k. Combined with the study of the empirical range given by Mesri and the test results, the P' was approximately 1.6 to 3.0 σ'_k, and $C_{\alpha max}$ appears near P' [41].

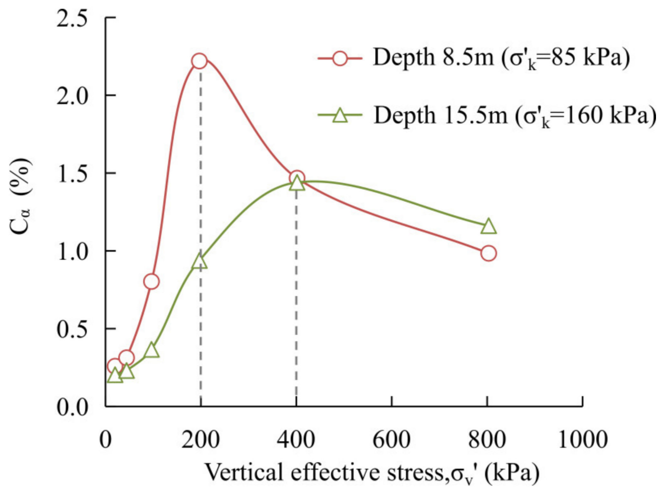

Figure 14. C_α at varied vertical effective stress σ_v' of Shanghai soft soil after [44].

Table 10. A summary of σ'_k and P' from different sites.

Site	Depth (m)	σ'_k (kPa)	P' (kPa)	P'/σ'_k
Nettoor, India [58]	1.5	35	100	2.9
	2.0	50	100	2.0
New Liskeard, Canada [50]	14.5	250	400	1.6
	30.0	410	800	2.0
Bothkennar, England [23]	5.2	43	100	2.3
Mexico City, Mexico [1]	15.0	180	400	2.2
Murro, Finland [59]	7.0	44	80	1.8
Saudi Arabia [60]	4.5	100	200	2.0
Ningbo, China [61]	8.5	80	200	2.5
	10.5	110	200	1.8
Shanghai, China [44]	8.5	85	200	2.4
	15.5	160	400	2.5
Tianjin, China [25]	6.0	60	100	1.7

As shown in Figure 15, when the vertical effective stress is smaller than σ'_k, it is called the pre-yield stage, and the C_α is small and slowly increases. When the vertical effective pressure exceeds σ'_k, the soil structure is destroyed, and the C_α increases rapidly with the pressure, and reaches the peak $C_{\alpha max}$ when the vertical effective pressure reaches P', which is the yield stage, and P' is approximately 1.6 to 3.0 times σ'_k. When the vertical effective pressure exceeds P' after severe structural damage, the C_α decreases and tends towards a stable value $C_{\alpha r}$, at which point the C_α is considered to be independent of the load.

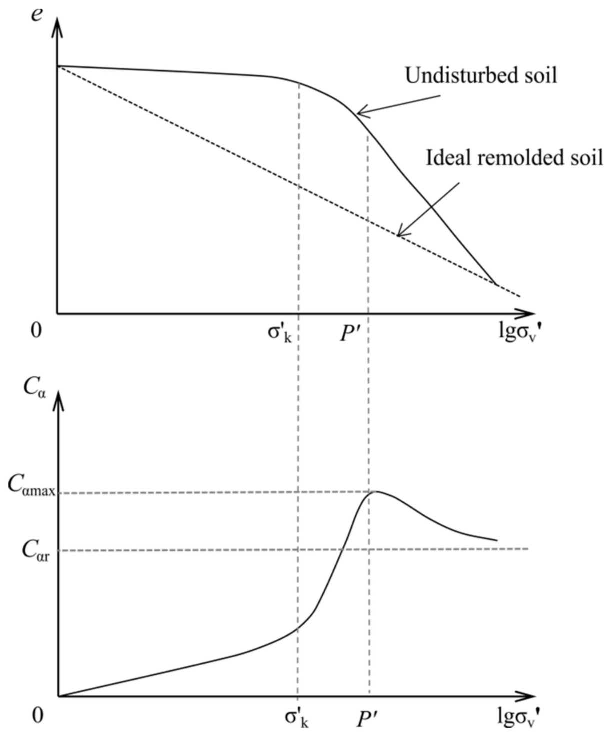

Figure 15. Variation of secondary compression coefficients with vertical effective stress.

4.5. Relationship between $C_{\alpha max}$ and Liquid Limit

It is known from one-dimensional consolidation creep tests that the $C_{\alpha max}$ for the soils in the four sites is in the vicinity of P', but the value of C_{α} is not related to the value of σ'_{k}. Cao found that the C_{α} of saturated clay changed linearly with increasing natural moisture content [6]. Although the natural moisture content of the SH was higher than that of TJ, the TJ had a higher C_{α} value than SH. According to the soil composition test of the five soft soils, the NB sample had higher clay and secondary mineral content, showing larger C_{α}. According to the test results, there is a good correspondence between $C_{\alpha max}$ and w_L. The w_L can be determined by the fall cone method using parallel samples. On this basis, natural clay test data from around the world, especially those from the coastal areas of Southeast Asia, were collected, and it was found that $C_{\alpha max}$ had a good linear relationship with the w_L, as shown in Figure 16 [1,9,12,16,23,50,55,58,59,61–75].

The liquid limit w_L is an important property of soil itself, indicating the maximum bound water content except free water that can be adsorbed by the clay. Xiao found that bound water is an important factor affecting the creep of soft soil [76]. Therefore, the bound water content adsorbed by soil has a significant influence on C_{α}. When the pressure is low, due to the large number of pores in the soil, the consolidation process of free water discharge with the least force of the grains is easy and fast, and the primary consolidation process is dominant. The creep degree is very low under this pressure state, and the C_{α} is small. In the primary consolidation process, free water and bound water are converted into free water, and the creep is mainly controlled by the bound water [77]. With increasing pressure and time, the primary consolidation effect becomes increasingly weak, the secondary compression increases and the value of C_{α} gradually increases. When the pressure reaches σ'_{k}, the damage of the soil structure is serious, the number of large pores is reduced, the small pores increase, the bound water content in the pores increases relatively, the degree of creep increases and the C_{α} value increases rapidly. The cohesion of the bound water is stronger than that of the free water and it has definite viscosity. The combination of the bound water strengthens the connection of the grains. With the gradual increase in pressure, the lower the combined water content, the greater the viscosity between the grains, and so the C_{α} of the soft soil reaches a peak at the maximum bound water content. Therefore, the liquid limit w_L can be used to predict the $C_{\alpha max}$ of soft soil. The soil with definite grain and mineral composition has a definite liquid limit, which reflects the influence of the soil composition on the secondary compression characteristics of soft soil.

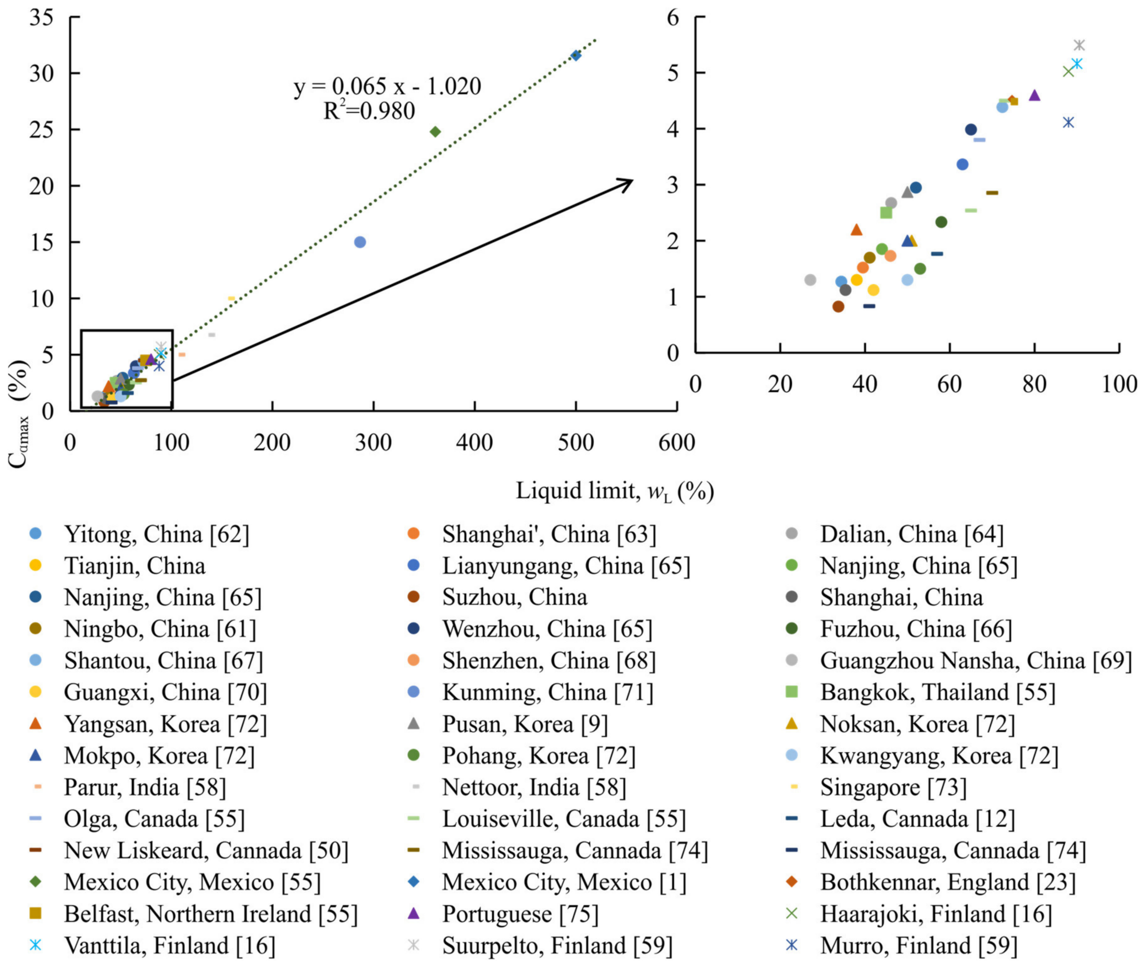

Figure 16. Relationship between $C_{\alpha max}$ and w_L.

5. Conclusions

According to the study of five kinds of natural sedimentary structural soils, which are from the SH site, TJ site, SZ site and NB site, it was found that the soil composition and structural characteristics of soft soil are important factors affecting soil compressibility.

1. The C_α/C_c values are 0.031, 0.034, 0.030 and 0.036 for the Shanghai, Tianjin, Suzhou and Ningbo soft soils, respectively, within the range of inorganic clays and silts given by Mesri. The C_α/C_c value of the Ningbo soft soil is the highest, which corresponds to its maximum compression index C_c. According to the compression index C_c obtained by compression test, C_α/C_c can be used to estimate the C_α.
2. According to the discussion of I_v and ΔI_v with pressure, the role of structure in the compression process is studied, when the pressure is greater than the structure yield stress σ'_k, the soil structure begins to break, and the ability of the natural sedimentary soft soil to resist the pressure is gradually weakened.
3. In the secondary compression process, the C_α varies with time. When σ_v' is less than σ'_k, it is in the pre-yield stage, the C_α is small and does not change much over time. The value of C_α is

significantly larger when $\sigma_v{}'$ is greater than σ'_k. The C_α decreases noticeably with time, finally tending to be stable, which fully reflects the progressive destruction process of the soil structure.

4. For natural sedimentary structural soil, soil structure has a significant influence on the variation pattern of the C_α. The soil structure resists the external pressure and hinders secondary compression, and structural damage is gradual. When the load is less than σ'_k, the structure is basically not destroyed, C_α is small; when the load exceeds σ'_k, the structure is gradually broken, and it completely yields at 1.6 to 3.0 times σ'_k, at this time the pressure is called the structure full yield stress P'. After the structure begins to break, the C_α gradually increases, and reaches the peak $C_{\alpha max}$ near P'; and there is an excellent correlation between $C_{\alpha max}$ and the liquid limit w_L. The $C_{\alpha max}$ is positively correlated with the bound water content of soft soil and reflects the influence of soil composition on the secondary compression characteristics of soft soil.

Author Contributions: N.J. contributed to the data analysis and manuscript writing. C.W. proposed the main structure of this study. Q.W. and S.L. provided useful advice and revised the manuscript. All authors have read and agreed to the published version of the manuscript.

Funding: This research was funded by the National Natural Science Foundation of China (No. 41572257) and (No. 41972267).

Acknowledgments: We are grateful to Jilin University for providing us with the experimental platform and anonymous reviewers for their valuable feedback on the manuscript.

Conflicts of Interest: The authors declare no conflict of interest.

References

1. Mesri, G.; Roskhsar, A.; Bohor, B.F. Composition and Compressibity of Typical Samples Mexico City Clay. *Geotechnique* **1975**, *25*, 527–554. [CrossRef]
2. Tanaka, H.; Locat, J.; Shibuya, S.; Soon, T.T.; Shiwakoti, D.R. Characterization of Singapore, Bangkok, and Ariake clays. *Can. Geotech. J.* **2001**, *38*, 378–400. [CrossRef]
3. CABR. *Specification for Geotechnical Investigation in Soft Clay Area*; China Building Industry Press: Beijing, China, 1992.
4. Zhao, C.G.; Bai, B.; Wang, Y.X. *Foundamentals of Soil Mechanics*; Tsinghua University Press: Beijing, China; Beijing Jiaotong University Press: Beijing, China, 2004.
5. Miao, L.C.; Kavazanjian, E. Secondary Compression Features of Jiangsu Soft Marine Clay. *Mar. Georesour. Geotechnol.* **2007**, *25*, 129–144. [CrossRef]
6. Cao, Y.P. Relationship of Coefficients of Secondary Consolidation with Moisture Content of Saturated Cohesive Soil. *China Harb. Eng.* **2007**, *149*, 21–23.
7. Xu, G.Z.; Yin, J. Compression Behavior of Secondary Clay Minerals at High Initial Water Contents. *Mar. Georesour. Geotechnol.* **2015**, *34*, 721–728. [CrossRef]
8. Park, J.H.; Koumoto, T. New Compression Index Equation. *J. Geotech. Geoenviron. Eng.* **2004**, *130*, 223–226. [CrossRef]
9. Suneel, M.; Park, L.K.; Im, J.C. Compressibility Characteristics of Korean Marine Clay. *Mar. Georesour. Geotechnol.* **2008**, *26*, 111–127. [CrossRef]
10. Alonso, E.E.; Navarro, V. Microstructural model for delayed deformation of clay: Loading history effects. *Can. Geotech. J.* **2005**, *42*, 381–392. [CrossRef]
11. Mesri, G.; Stark, T.D.; Ajlouni, M.A.; Chen, C.S. Secondary compression of peat with or without surcharging. *J. Geotech. Eng. Div. ASCE* **1997**, *123*, 411–421. [CrossRef]
12. Mesri, G.; Godlewski, P.M. Time and stress compressibility interrelationship. *J. Geotech. Eng. Div. ASCE* **1977**, *103*, 417–430.
13. Mesri, G. Primary Compression and Secondary Compression. In Proceedings of the Symposium on Soil Behavior and Soft Ground Construction Honoring Charles C. "Chuck" Ladd, Cambridge, MA, USA, 5–6 October 2001; Volume 119, pp. 122–166.
14. Yin, Z.Y.; Chang, C.S. Non-uniqueness of critical state line in compression and extension conditions. *Int. J. Numer. Anal. Methods Geomech.* **2009**, *33*, 1315–1338. [CrossRef]

15. Karstunen, M.; Yin, Z.Y. Modelling time-dependent behaviour of Murro test embankment. *Géotechnique* **2010**, *60*, 735–749. [CrossRef]
16. Yin, Z.Y.; Karstunen, M.; Chang, C.S.; Koskinen, M.; Lojander, M. Modeling Time-Dependent Behavior of Soft Sensitive Clay. *J. Geotech. Geoenviron. Eng.* **2011**, *137*, 1103–1113. [CrossRef]
17. Di Maio, C.; Santoli, L.; Schiavone, P. Volume change behaviour of clays: The influence of mineral composition, pore fluid composition and stress state. *Mech. Mater.* **2004**, *36*, 435–451. [CrossRef]
18. Voltolini, M.; Wenk, H.R.; Mondol, N.H.; Bjørlykke, K.; Jahren, J. Anisotropy of experimentally compressed kaolinite-illite-quartz mixtures. *Geophysics* **2009**, *74*, D13–D23. [CrossRef]
19. Horpibulsuk, S.; Yangsukkaseam, N.; Chinkulkijniwat, A.; Du, Y.J. Compressibility and permeability of Bangkok clay compared with kaolinite and bentonite. *Appl. Clay Sci.* **2011**, *52*, 150–159. [CrossRef]
20. Bjerrum, L. Engineering geology of Norwegian normally consolidated marine clays as related to the settlements of buildings. *Géotechnique* **1967**, *17*, 83–118. [CrossRef]
21. Newland, P.L.; Allely, B.H. A study of the consolidation characteristics of a clay. *Géotechnique* **1960**, *10*, 62–74. [CrossRef]
22. Horn, H.M.; Lambe, I.W. Settlement of buildings on the MIT campus. *J. Soil Mech. Found. Div.* **1964**, *90*, 181–196.
23. Nash, D.F.T.; Davison, L.R.; Sills, G.C. One-dimensional consolidation testing for soft clay from Bothkennar. *Géotechnique* **1992**, *42*, 241–256. [CrossRef]
24. Liu, S.M.; Zeng, G.X. Secondary Consolidation Deformation Characteristics of Soft Clay. *J. Zhejiang Univ. (Nat. Sci.)* **1990**, *24*, 840–848.
25. Lei, H.Y. Study on secondary consolidation deformation characteristics of soft soil in Tianjin. *J. Eng. Geol.* **2002**, *10*, 385–390.
26. Yin, Z.Z.; Zhang, H.B.; Zhu, J.G. Secondary consolidation of soft soils. *Chin. J. Geotech. Eng.* **2003**, *25*, 521–526.
27. Mitchell, J.K. Practical problems from surprising soil Behavior. *J. Geotech. Eng.* **1986**, *112*, 255–289. [CrossRef]
28. Chandler, R.J. Clay sediments in depositional basin: The geotechnical cycle. *Q. J. Eng. Geol. Hydrol.* **2000**, *33*, 7–39. [CrossRef]
29. Hong, Z.; Liu, H.; Chang, N. Critical state sedimentation line of soft marine clays. *China Ocean Eng.* **2003**, *17*, 631–640.
30. Schmertmann, J.H. The mechanical aging of soils. *J. Geotech. Eng.* **1991**, *117*, 1288–1330. [CrossRef]
31. Leroueil, S.; Vaughan, P.R. The general and congruent effects of structure in natural soils and weak rocks. *Géotechnique* **1990**, *40*, 281–284. [CrossRef]
32. Leroueil, S.; Roy, M.; La Rochelle, P.; Brucy, F.; Tavenas, F. Behavior of Destructured Natural Clays. *J. Geotech. Eng. Div. ASCE* **1979**, *105*, 759–778.
33. Hattab, M.; Hammad, T.; Fleureau, J.M.; Hicher, P.Y. Behaviour of a sensitive marine sediment: Microstructural investigation. *Geotechnique* **2013**, *63*, 71–84. [CrossRef]
34. Shen, Z.J. The Mathematical Model of Soil Structure-The Core Problem of Soil Mechanics in the 21st Century. *Chin. J. Geotech. Eng.* **1996**, *18*, 95–97.
35. Perisic, G.A.; Ovalle, C.; Barrios, A. Compressibility and creep of a diatomaceous soil. *Eng. Geol.* **2019**, *258*, 105145. [CrossRef]
36. Hong, Z.S.; Tateishi, Y.; Jie, H. Experimental Study of Macro and Micro behavior of Natural Diatomite. *J. Geotech. Geoenviron.* **2006**, *132*, 603–610. [CrossRef]
37. Shen, Z.J. Engineering properties of soft soils and design of soft ground. *Chin. J. Geotech. Eng.* **1998**, *20*, 100–111.
38. Yang, C.; John, P.C.; Sheng, D.C. Description of compression behaviour of structured soils and its application. *Can. Geotech. J.* **2014**, *51*, 921–933. [CrossRef]
39. Burland, J.B. On the compressibility and shear strength of natural clays. *Géotechnique* **1990**, *40*, 329–378. [CrossRef]
40. Hong, Z.S.; Onitsuka, K. A method of correcting yield stress and compression index of Ariake clays for sample disturbance. *Soils Found.* **1998**, *38*, 211–222. [CrossRef]
41. Mesri, G.; Choi, Y.K. Discussion of “Time effects on the stress-strain behaviours of natural soft clays”. *Géotechnique* **1984**, *34*, 439–442.
42. Shao, G.H.; Liu, S.Y. Research on secondary consolidation of structural marine clays. *Rock Soil Mech.* **2008**, *29*, 2057–2062.

43. Zhang, X.W.; Wang, C.M. Effect of soft clay structure on secondary consolidation coefficient. *Rock Soil Mech.* **2012**, *33*, 476–483.
44. Li, Q.; Ng, C.W.W.; Liu, G.B. Low secondary compressibility and shear strength of Shanghai Clay. *J. Cent. South Univ.* **2012**, *19*, 2323–2332. [CrossRef]
45. Zeng, L.L.; Hong, Z.S.; Liu, S.Y. A method for predicting deformation caused by secondary consolidation for naturally sedimentary structural clays. *Rock Soil Mech.* **2011**, *32*, 3136–3142.
46. Ministry of Construction. *Code for Investigation of Geotechnical Engineering*; GB 50021-2001; China Building Industry Press: Beijing, China, 2002.
47. British Standard Institution. *The Code of Practice for Site Investigations*; BS 5930; British Standard Institution: London, UK, 1999.
48. Sun, J. *Rheology and Engineering Application of Geomaterials*; Beijing Building Industry Press: Beijing, China, 1999.
49. Deng, Z.B. Research and Application of Soft Clay Creep Test and Constitutive Model Identification Method. Ph.D. Thesis, Central South University, Hunan, China, 2007.
50. Quigley, R.M.; Ogunbadejo, T.A. Clay Layer Fabric and oedometer consolidation of a soft varved Clay. *Can. Geotech. J.* **1972**, *9*, 165–175. [CrossRef]
51. Schmertmann, J.M. The undisturbed consolidation behavior of clay. *Trans. ASCE* **1955**, *120*, 1201–1211.
52. Li, T.; Qian, Y.S. Evaluation of soil sample disturbance and determination of pre-consolidation pressure. *J. Geotech. Eng.* **1987**, *5*, 21–30.
53. Zou, Y.Q.; Wang, Y.B.; Shao, M.X. A stepwise approximation of the preconsolidation pressure. *J. Geotech. Eng.* **1994**, *160*, 54–61.
54. Crawford, C.B. Interpretation of the consolidation test. *J. Soil Mech. Found. Div.* **1964**, *90*, 87–102.
55. Bell, A.L.; Graham, J.; Crooks, J.H.A. Time effects on the stress–strain behaviour of natural soft clays. *Géotechnique* **1983**, *33*, 327–340.
56. Berre, T.; Iversen, K. Oedometer tests with different specimen heights on a clay exhibiting large secondary compression. *Géotechnique* **1972**, *22*, 53–70. [CrossRef]
57. Leroueil, S.; Kabbaj, M.; Tavenas, F.; Bouchard, R. Stress–strain–strain rate relation for the compressibility of sensitive natural clays. *Géotechnique* **1985**, *35*, 159–180.
58. Jose, B.T.; Sridharan, A.; Abraham, B.M. A study of geotechnical properties of Cochin Marine Clays. *Mar. Geotech.* **1988**, *7*, 189–209. [CrossRef]
59. Stapelfeldt, T.; Lojander, M.; Vepaslainen, P. Determination of horizontal permeability of soft clay. In Proceedings of the 17th International Conference on Soil Mechanics and Foundation Engineering, Madrid, Spain, 3 January 2007; pp. 1385–1389.
60. Al-Shamrani, M.A. Application of the C_α/C_c concept to secondary compression of sabkha soils. *Can. Geotech. J.* **1998**, *35*, 15–26. [CrossRef]
61. Feng, Z.G.; Zhu, J.G. Experimental study on secondary consolidation behavior of soft soils. *J. Hydraul. Eng.* **2009**, *40*, 583–588.
62. Wang, C.M.; Zhang, S.Y.; Li, S. Characteristics of Secondary Consolidation of Yitong Soft Soil. *J. Jilin Univ. (Earth Sci.)* **2018**, *48*, 799–804.
63. Xu, S.; Chen, Y.L.; Zhao, C.X. One-dimensional consolidation tests of creep deformation and secondary consolidation characteristics of soft soils in shanghai area. *J. Eng. Geol.* **2008**, *16*, 495–501.
64. Jiang, M.J.; Liu, J.D.; Yin, Z.Y. Consolidation and creep behaviors of two typical marine clays in China. *China Ocean Eng.* **2014**, *28*, 629–644. [CrossRef]
65. Zeng, L.L. Deformation Mechanism and Structural Compression Model of Natural Sedimentary Soft Clay. Ph.D. Thesis, Southeast University, Jiangsu, China, 2010.
66. Chen, Z.; Kong, Q. Experimental study on secondary consolidation properties of Fuzhou soft soils. *J. Cent. South Univ.* **2014**, *45*, 3602–3607.
67. Yu, X.J.; Yin, Z.Z.; Dong, W.J. Influence of load on secondary consolidation deformation of soft soils. *Chin. J. Geotech. Eng.* **2007**, *29*, 913–916.
68. Zhang, H.M.; Zhang, D.K. Secondary Consolidation Deformation Characteristics of Soft Soil in Shenzhen. In Proceedings of the 7th Conference of Soil Mechanics and Basic Engineering of China Civil Engineering Society, Xi'an, China, 25–29 October 1994; pp. 97–100.

69. Zhou, Q.J.; Chen, X.P. Experimental study on creep characteristics of soft soils. *Chin. J. Geotech. Eng.* **2006**, *28*, 626–630.
70. Shi, X.C.; Wang, R.; Hu, Y.Y. Research on deformation characteristics of marine silt. *J. Yangtz River Sci. Res. I.* **2003**, *20*, 17–18.
71. Gui, Y.; Yu, Z.H.; Liu, H.M.; Cao, J. Secondary consolidation properties and mechanism of plateau lacustrine peaty soil. *Chin. J. Geotech. Eng.* **2015**, *37*, 1390–1398.
72. Suneel, M.; Konni, G.R.; Chul, I.J. Secondary Compression Index Equation for Soft Clays. *Geotech. Geol. Eng.* **2017**, *17*, 358. [CrossRef]
73. Tan, J.L.; Leong, E.C.; Rahardjo, H. Compressibility characteristics of peaty soils. In Proceedings of the Third International Conference on Soft Soil Engineering, Hong Kong, China, 6–8 December 2001; pp. 689–694.
74. Iyer, B. Discussion of "C_α/C_c Concept and K_0 during Secondary Compression" by G. Mesri and A. Castro. *J. Geotech. Eng.* **1989**, *115*, 263–264. [CrossRef]
75. Coelho, P.A.L.F.; Lemos, L.J.L. Compressibility characteristics of a Portuguese soft deposit. In Proceedings of the Third International Conference on Soft Soil Engineering, Hong Kong, China, 6–8 December 2001; pp. 663–668.
76. Xiao, S.F.; Fang, H.G.; Wang, Q. Creep behavior of combined water and consolidation in soft soils. *J. Eng. Geol.* **2014**, *4*, 1464–1469.
77. Zhang, X.W.; Wang, C.M.; Li, J.X. Experimental study of coupling behaviors of consolidation-creep of soft clay and its mechanism. *Rock Soil Mech.* **2011**, *32*, 3584–3590.